
**AFRL-AFOSR-UK-TR-2023-0033**

# Exploiting low-dimensional properties of carbon nanotubes in macroscopic yarns for charge transfer and storage (NANOYARN)

**Vilatela, Juan**
**FUNDACION IMDEA MATERIALES**
**CALLE DE ERIC KANDEL, 2**
**GETAFE, , 28906**
**ESP**

**12/14/2022**
**Final Technical Report**



Air Force Research Laboratory
Air Force Office of Scientific Research
European Office of Aerospace Research and Development
Unit 4515 Box 14, APO AE 09421

# REPORT DOCUMENTATION PAGE

**PLEASE DO NOT RETURN YOUR FORM TO THE ABOVE ORGANIZATION.**

| 1. REPORT DATE | 2. REPORT TYPE | 3. DATES COVERED | |
|---|---|---|---|
| 20221214 | Final | START DATE<br>20180815 | END DATE<br>20220814 |

**4. TITLE AND SUBTITLE**
Exploiting low-dimensional properties of carbon nanotubes in macroscopic yarns for charge transfer and storage (NANOYARN)

| 5a. CONTRACT NUMBER | 5b. GRANT NUMBER | 5c. PROGRAM ELEMENT NUMBER |
|---|---|---|
| | FA9550-18-1-7016 | |
| **5d. PROJECT NUMBER** | **5e. TASK NUMBER** | **5f. WORK UNIT NUMBER** |
| | | |

**6. AUTHOR(S)**
Juan Vilatela

| 7. PERFORMING ORGANIZATION NAME(S) AND ADDRESS(ES) | 8. PERFORMING ORGANIZATION REPORT NUMBER |
|---|---|
| FUNDACION IMDEA MATERIALES<br>CALLE DE ERIC KANDEL, 2<br>GETAFE 28906<br>ESP | |

| 9. SPONSORING/MONITORING AGENCY NAME(S) AND ADDRESS(ES) | 10. SPONSOR/MONITOR'S ACRONYM(S) | 11. SPONSOR/MONITOR'S REPORT NUMBER(S) |
|---|---|---|
| EOARD<br>UNIT 4515<br>APO AE 09421-4515 | AFRL/AFOSR IOE | AFRL-AFOSR-UK-TR-2023-0033 |

**12. DISTRIBUTION/AVAILABILITY STATEMENT**
A Distribution Unlimited: PB Public Release

**13. SUPPLEMENTARY NOTES**

**14. ABSTRACT**
This final report covers work performed between August 2018 and August 2022 for the project 'Exploiting low-dimensional properties of carbon nanotubes in macroscopic yarns for charge transfer and storage', funded by the Air Force Office of Scientific Research (AFOSR).

Overall, the project has led to a new family of continuous intercalation compounds with unprecedented long-range order, a combination of bulk mechanical and electrical properties beyond those of traditional high-performance materials, and the prospect of realising new physical properties in macroscopic fibres of metamaterials beyond the carbon nanotube intercalation compounds studied in NANOYARN. Through study of different carbon nanotube fibre model systems we were able to clarify the role of the structure of constituent CNTs and their macromolecular organisation in the formation of intercalation compounds with acceptor materials (Fe3Cl and Br). A revised method is proposed to determine charge transfer between host and intercalate, and estimate its spatial distribution in the CNT layers based on Raman spectroscopy using multiple laser lines. The project also studied the relation between bulk tensile properties and electrical conductivity (including at cryogenic temperatures), and the structure of the intercalation compound in terms of inter-tube separation and the supramolecular arrangement of the intercalate. Provided the intercalate preserves the structure of constituent bundles, tensile properties remain largely unaltered, which fundamentally contrast with conventional layered intercalation graphite compounds. Intercalate charged species (e.g. tribromide ion) reduce resistance for transverse electron transfer between adjacent CNTs, increasing overall conductivity to the level approaching Cu. Details of the results of the project are included mainly in five scientific publications and a PhD thesis.

**15. SUBJECT TERMS**

| 16. SECURITY CLASSIFICATION OF: | | | 17. LIMITATION OF ABSTRACT | 18. NUMBER OF PAGES |
|---|---|---|---|---|
| a. REPORT<br>U | b. ABSTRACT<br>U | c. THIS PAGE<br>U | SAR | 19 |

| 19a. NAME OF RESPONSIBLE PERSON | 19b. PHONE NUMBER *(Include area code)* |
|---|---|
| DAVID SWANSON | 785-6565 |

# NANOYARN

**Exploiting low-dimensional properties of carbon nanotubes in macroscopic yarns for charge transfer and storage**

***AWARD NO: FA9550-18-1-7016***

***PRINCIPAL INVESTIGATOR: Juan José Vilatela***

# FINAL REPORT

(08/15/2018 - 08/14/2022)

*"This material is based upon work supported by the Air Force Office of Scientific Research under award number FA9550-18-1-7016."*



- Federal Agency and Organizational Element to Which Report is Submitted: AFOSR(Air Force Office of Scientific Research)
- Federal Grant or Other Identifying Number Assigned by Federal Agency: Fundación IMDEA Materiales (IMDEA)
- DUNS Number: 460033493
- EIN: G84908953

**For more information on this document or NANOYARN, please contact:**

Dr. Juan José Vilatela
juanjose.vilatela@imdea.org
Fundación IMDEA Materiales
Eric Kandel, 2
Parque Científico y Tecnológico - Tecnogetafe
28906 Getafe (Madrid) SPAIN
Tel: +34 91 549 3422 / Fax: +34 91 550 3047
http://www.materials.imdea.org/

# TABLE OF CONTENTS

# 1 SUMMARY

This final report covers work performed between August 2018 and August 2022 for the project 'Exploiting low-dimensional properties of carbon nanotubes in macroscopic yarns for charge transfer and storage', funded by the Air Force Office of Scientific Research (AFOSR).

Overall, the project has led to a new family of continuous intercalation compounds with unprecedented long-range order, a combination of bulk mechanical and electrical properties beyond those of traditional high-performance materials, and the prospect of realising new physical properties in macroscopic fibres of metamaterials beyond the carbon nanotube intercalation compounds studied in NANOYARN. Through study of different carbon nanotube fibre model systems we were able to clarify the role of the structure of constituent CNTs and their macromolecular organisation in the formation of intercalation compounds with acceptor materials ($Fe_3Cl$ and Br). A revised method is proposed to determine charge transfer between host and intercalate, and estimate its spatial distribution in the CNT layers based on Raman spectroscopy using multiple laser lines. The project also studied the relation between bulk tensile properties and electrical conductivity (including at cryogenic temperatures), and the structure of the intercalation compound in terms of inter-tube separation and the supramolecular arrangement of the intercalate. Provided the intercalate preserves the structure of constituent bundles, tensile properties remain largely unaltered, which fundamentally contrast with conventional layered intercalation graphite compounds. Intercalate charged species (e.g. tribromide ion) reduce resistance for transverse electron transfer between adjacent CNTs, increasing overall conductivity to the level approaching Cu. Details of the results of the project are included mainly in five scientific publications and a PhD thesis.

# 2 INTRODUCTION

The assembly of long highly crystalline nanocarbons into continuous arrays has led to a paradigmatic change in materials science. These arrays can be visualised as macroscopic networks of constituent molecules (a CNT or graphene layer) with superlative properties (highest in-plane stiffness, carrier mobility), with large possibilities to tailor assembly in terms of molecular orientation. Thus, assembling CNT parallel to other as a fibre results in a high-performance fibre, with reports showing tensile strength/stiffness similar to CF[1], superior fracture energy than Kevlar[2], similar electrical and thermal conductivity as Cu[3].

The intercalation of ions between CNTs is an attractive method to introduce donors/acceptors into the material with minimum bond breakage. Because of the weak interaction between layers in graphite, graphitic materials are ideal hosts for intercalation compounds. Indeed, the insertion mechanism and physical properties in graphite intercalation compounds (GIC) have received vast attention over several decades[4]. The fascination with GIC stems from the large reversible changes in physical properties produced by highly controlled intercalation, resulting from lattice distortion and the introduction of a large concentration of free carriers in a system with high carrier mobility but an intrinsically low density of free carriers.

The objectives of the project are 1) to understand the mechanisms that govern gas phase intercalation in carbon nanotube (CNT) fibres, 2) to determine the effect of intercalants on bulk fibre properties, particularly longitudinal electrical conductivity and tensile mechanical properties and 3) to perform preliminary measurements on low-dimensional properties of intercalated CNT fibres.

# 3 METHODS, ASSUMPTIONS AND PROCEDURES

The project used two classes of CNT fibres: a) samples produced in house through floating catalyst chemical vapour deposition, which are polydisperse in terms of the distribution of CNT layers and diameters and which have a moderate degree of alignment (azimuthal FWHM ≈ 15°); and b) fibres from liquid crystalline solutions, which are nearly monodisperse and have high alignment (azimuthal FWHM ≈ 6°).

Intercalation was conducted using the two-zone vapour transport technique. First, sample and intercalant are introduced in a tubular glass capsule in an argon atmosphere in a glove box. The system is subsequently sealed at a low vacuum ($\sim 10^{-2}$ mbar). The capsule is then placed in a temperature control rig. Exposure to vapour is maintained for extended periods from several hours to a couple of days.

Wide-angle x-ray scattering (WAXS) measurements were performed under microfocus configuration at the NCD-SWEET beamline of ALBA synchrotron. Multiple patterns were collected in each measurement in order to reduce noise. The presented patterns result from

azimuthal integration of the 2D WAXS data after averaging and background subtraction. Coherent lengths, equivalent to crystal sizes, are calculated with Scherrer equation, using the proportionality factors employed in graphite. No instrumental broadening correction is required due to the high coherence of synchrotron radiation. In-plane crystal size, La, is obtained with the FWHM of the (100) peak, fitted with a split Pearson VII function. For graphitised samples, there is evidence of an additional peak, identified as the (101) reflection. For those samples, La is calculated from the (100) after deconvolution. Out-of-plane crystal size, Lc, is obtained through Scherrer equation using the (002) peak, fitted with a pseudo-Voigt function.

Raman spectra were collected with 532nm and 785nm laser lines, using low power and 10s exposure to avoid sample heating. The laser polarisation was parallel to the fibre axis to increase scattering intensity.

# 6 RESULTS AND DISCUSSION

The project studied intercalation of two different types of host materials. In its first half, the focus was on fibres produced through at IMDEA Materials through floating catalyst chemical vapour deposition (FCCVD). They are characterised by a moderate degree of alignment, hence relatively high porosity (25%) and a wide distribution of CNT diameters. The second half of NANOYARN dealt with commercial CNT fibres produced through liquid-crystal spinning and which have near-perfect alignment and quasi-monodisperse diameter distribution. The main results are summarised in the following three publications:

*Macroscopic yarns of FeCl3-intercalated collapsed carbon nanotubes with high doping and stability*. **Carbon 173**, 311-321, 2021. DOI: **10.1016/j.carbon.2020.10.052**

*Ultrahigh strength, modulus, and conductivity of graphitic fibers by macromolecular coalescence*. **Science Advances 8 (16)**, 2022. DOI: **10.1126/sciadv.abn0939**

*Continuous intercalation compound fibers of bromine wires and aligned CNTs for high-performance conductors*. **Carbon**, under review.

Other publications produced in the project are:

*Improved alignment and stress transfer in CNT fibre fabrics studied by in situ X-ray and Raman during wet-drawing*. **Carbon** , 2022. DOI: **10.1016/j.carbon.2022.06.045**

*Suspended nanomaterial synthesis via floating catalyst and direct assembly as networks for high-performance applications*. **Nanoscale**, under review.

### 6.1 IMDEA fibres of collapsed CNTs

This material used for intercalation consists of continuous fibres made up of long bundles of collapsed (i.e., flattened) CNTs stacked in graphitic-like domains. Figure 1 presents examples of transmission electron micrographs showing their bundle structure, composed of mainly 2-4 wall collapsed CNTs stacked turbostratically into graphitic ribbon-like structures. The largest bundles

contain around 15-45 flattened nanotubes, forming stacks ~10-30 nm thick. The mean width of the collapsed CNTs is ~15 nm. Seen as a graphitic crystal, the collapsed CNTs bundles form very long domains with no grain boundaries (tubes length is hundreds of microns) offering large graphitic areas to host and stabilise intercalants. Overall, with the view of forming intercalation compounds, this system has structural attributes distinct from graphite. The sp2 carbon layers have very large in-plane crystallite size, but with a relatively low interlayer binding energy due to turbostratic stacking. In addition, the elongated crystals offer lateral access to the intercalant.

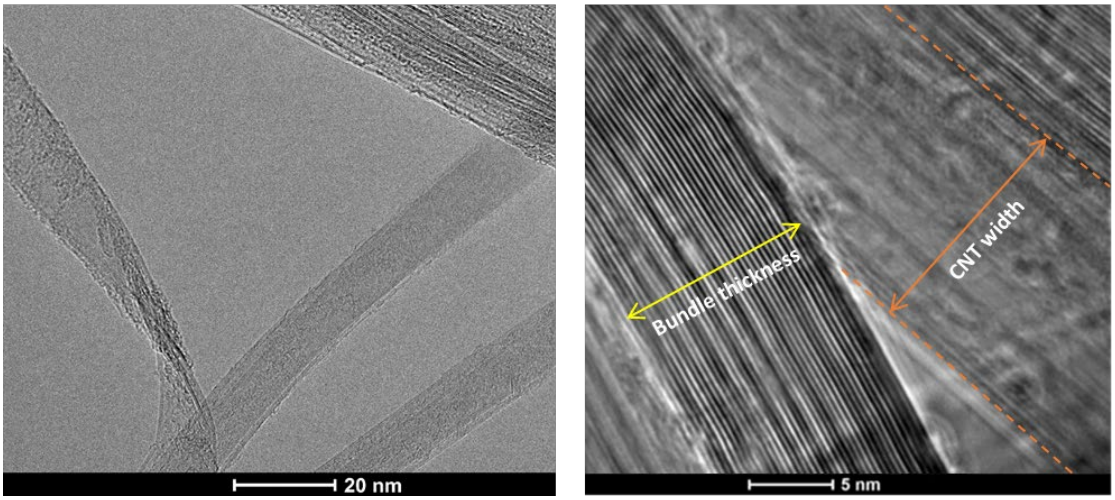


Figure 1. a) HRTEM image of a bundle composed of few double walled collapsed CNTs in which one “tube” is detached. As it twists over itself, we are able to observe that is not rounded, but planar. b) HRTEM micrograph showing two bundles of collapsed CNTs forming highly graphitic stacked domains. The mean width of the collapsed tubes composing the sample is around 15 nm, as the one observed in the tubes in a) and b).

Iron (III) chloride (FeCl3) was used for intercalation in these flattened structures. Metal halides have the highest degree of charge transfer among all p-type dopants[5] and can lead to stable intercalation compounds depending on the degree of graphitization of the carbon layers.[6–8] The fibres of collapsed CNTs were intercalated with $FeCl_3$ using the two-zone method.[9,10] The ribbon-like structure of the collapsed CNT bundles enables direct observation of intercalation domains by transmission electron microscopy (TEM) imaging, which provides extraordinary new insight into the structure of the intercalated system. Several aspects of the morphology of the intercalated compound are shown in Figure 2. The extension of the intercalated $FeCl_3$ monolayers is large, as observed in Figure 2a; lengths of over 200 nm are found throughout the CNT fibre material. Intercalated regions are readily distinguished in TEM micrographs due to the highly increased distance between carbon planes. The distance between neighbouring collapsed CNTs when a $FeCl_3$ monolayer is intercalated increases typically from ~3.45 Å to ~9.4 Å (see inset in Figure 2.a), which corresponds closely to the separation observed in $FeCl_3$-GICs.[4,11] A separation of 11.5 Å is also observed in some regions, which is due to the conversion of $FeCl_3$ into FeClO at some of the edges.

Although intercalated $FeCl_3$ predominates as a monolayer, interestingly, there are some areas intercalated with multilayer crystals of $FeCl_3$. Figure 2c shows examples of domains with 5 layers of $FeCl_3$ intercalated between CNTs. A closer inspection of an intercalation edge (Figure 2b)

shows a terrace-like structure, suggesting that multilayer crystals are formed over an already intercalated $FeCl_3$ monolayer, i.e., once the carbon planes had already been separated. In this scenario, entry of a new $FeCl_3$ nucleus in an intercalated region does not require overcoming the van der Waals interaction between carbon planes, but only the interaction between the charged $FeCl_3$ and sp2 carbon layers, in addition to the strain energy from CNT deformation. HRTEM observation also shows that multilayers of $FeCl_3$ are highly crystalline and have crystallographic registry. The example in Figure 2.c shows dark field images of basal planes (003) parallel to the CNTs, and interplanar diffraction from (2-13) and (2-1-3). The corresponding crystal orientation is shown as inset in Figure 2c.

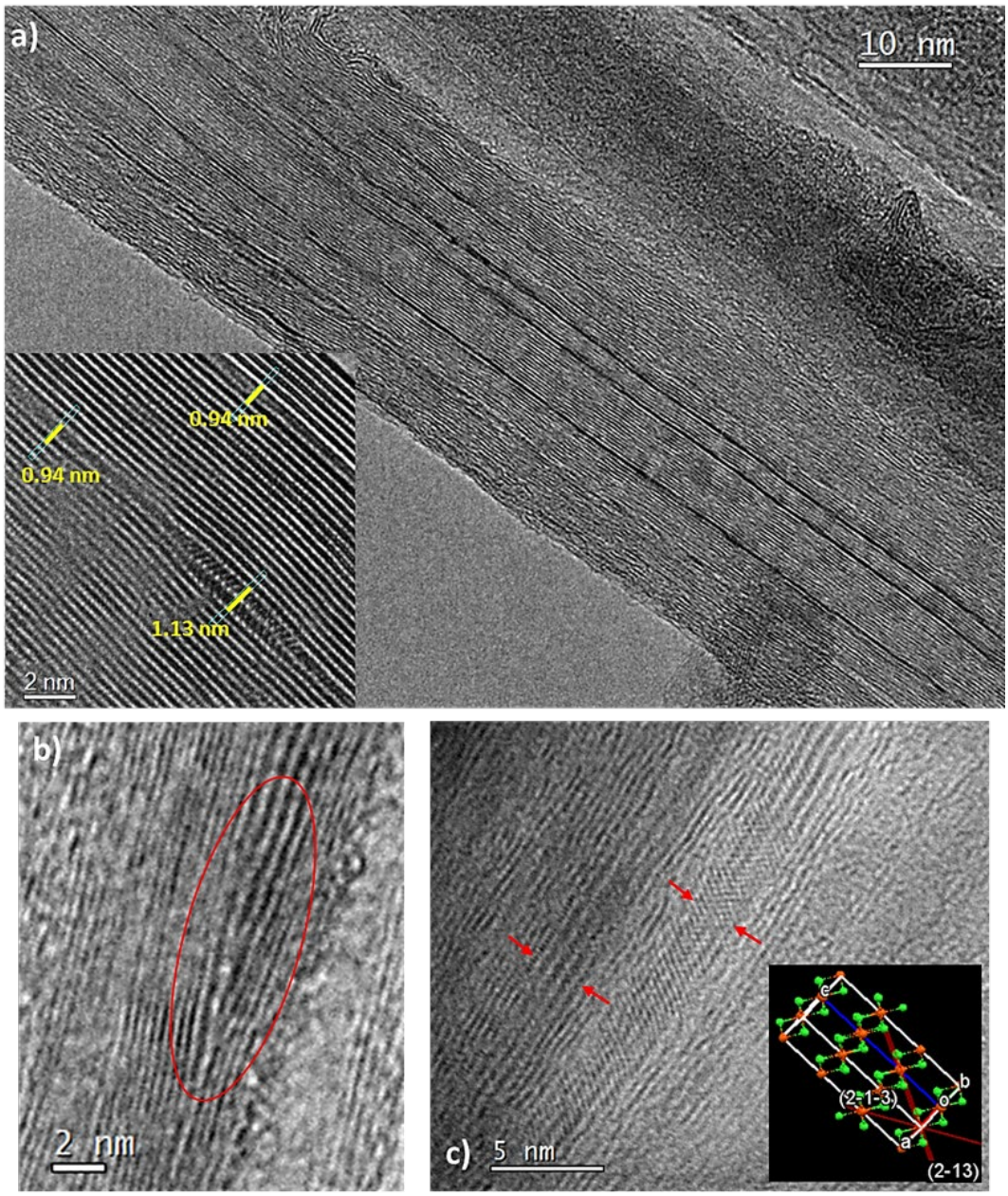


Figure 2. HRTEM micrographs of a sample of $FeCl_3$-intercalated collapsed CNT fibre with minimised exposure to air. a) Long intercalated regions appear, observed as dark stripes in domains with an increased distance between graphitic planes b) Multilayers of ferric chloride

appear intercalated between consecutive collapsed nanotubes. An intercalated monoloayer can act as a wedge that favours the formation of multiple layers of intercalant. c) Multilayers of intercalant are have crystallographic registry between layers, as confirmed by interlayer features in the FFT of the interference pattern, and illustrated in the schematic.

Based on the observed intercalant morphology and bundle structure, we envisage an intercalation process in similar steps as $FeCl_3$-GICs, but with faster intercalation kinetics. First, $FeCl_3$ clusters adsorb on the lateral (exposed) face of the CNTs. A $FeCl_3$ nucleus enters as a monolayer between the collapsed CNTs, overcoming the van der Waals interaction between collapsed CNTs through electron transfer to $FeCl_3$. Entry of the $FeCl_3$ nucleus acts as a wedge, forming a separation between CNTs that propagates laterally beyond the initial nucleus size because of the high in-plane stiffness of the CNTs. Bundle wedging is favored by the relatively small bundle thickness; in graphite, for example, high compaction of graphitic planes in a monolithic structure difficult their separation, forcing the intercalation process to start by the uppermost layers.[12] Furthermore, the inherently turbostratic stack makes the separation forces required for intercalation lower compared to AB stacked graphites. Once the wedge is created, the opening between collapsed CNTs is readily accessible for further lateral entry of $FeCl_3$, thus leading to longitudinal growth of the intercalated domain. The absence of defective edges (usually present in graphites) and high quantity of exposed faces where nucleus can be formed surely leads to a higher intercalation kinetics.[13]

### 6.2 Charge transfer in $FeCl_3$/collapsed CNT fibres

Charge transfer between $FeCl_3$ and the CNTs was confirmed through various spectroscopic techniques, and Raman spectroscopy enabled accurate determination of the charge transferred and estimation of the distribution of charge in the different CNT layers. The Raman spectra of pristine and intercalated collapsed CNTs is shown in Figure 3 for excitation wavelengths of 532 nm and 785 nm. The G-band of the intercalated sample is composed of two main contributions (as in stage>2 GICs): one from the sp2 carbon layers next to the intercalant, usually called bounding layers, and the other from the interior layers, where a lower degree of charge transfer occurs.[14–16] A large upshift is the G band is found upon $FeCl_3$ intercalation. $\Delta G_{bounding}$ ~25 $cm^{-1}$ for both laser wavelengths, while $\Delta G_{interior}$ is ~11 $cm^{-1}$ for the 532 nm laser and ~6 $cm^{-1}$ for the 785 nm excitation.

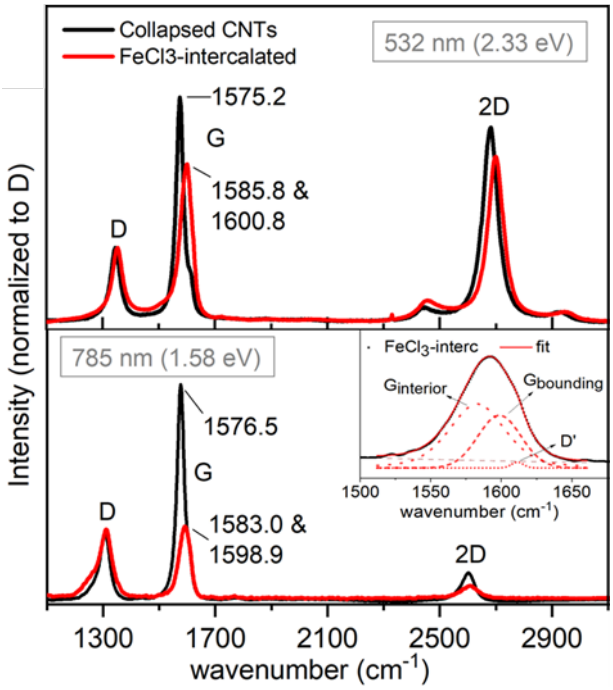


Figure 3. Raman spectra of the pristine and $FeCl_3$-intercalated col-lapsed CNT fibres taken at excitation wavelengths of: a) 532 nm (2.34 eV), and b) 785 nm (1.58 eV). All patterns are normalized to the D peak maximum intensity. In a) the 2D over D ratio remain fairly equal after intercalation, showing that no further defects are introduced in the intercalation pro-cess. The apparent loss in resonance and increase in FWHM of the G peak comes from the split of the band in two contribution.

Drawing from recent work on graphene[17,18], we use the relation between G and 2D Raman peak position to separate dynamical and strain shifts, and then calculate their contributions to total charge transfer to each CNT layer. These effects can be visually distinguished through their different slopes in a plot of G vs 2D position: uniaxial strain effects produce shifts resulting in a peak position ratio of 2D/G = 2.2, whereas dynamic effects give a smaller ratio of 0.75 [17],[18]. To determine charge transferred from the Raman shift components, we note that in graphitic systems the deformation of the graphene layers upon electron transfer to the intercalant behaves as a hydrostatic pressure, with G scaling linear with *f;* this component is analogous to a gate voltage. On the other hand, the dynamic part scales as the square root of *f* [19].

$$\Delta G = af + b\sqrt{f}$$

$$\Delta G = \Delta G_{strain} + \Delta G_{dynamic} = 580 \cdot f + 140 \cdot f^{1/2}$$

This gives $f = 0.013$, equivalent to a surface electron concentration of ~5·10^13 $cm^{-2}$ for the outer layer or a molecule of $FeCl_3$ per 77 carbon atoms. Finally, we use expressions derived from density functional theory simulations[20,21] to determine to the a change in Fermi level of

$\Delta E_F = -6.04 \cdot \sqrt{f} = -0.68\, eV$. This method to calculate charge transfer is significantly more accurate than under previous assumptions in the field (Figure 4b), and will be of broader use in the study of intercalated nanocarbon materials.

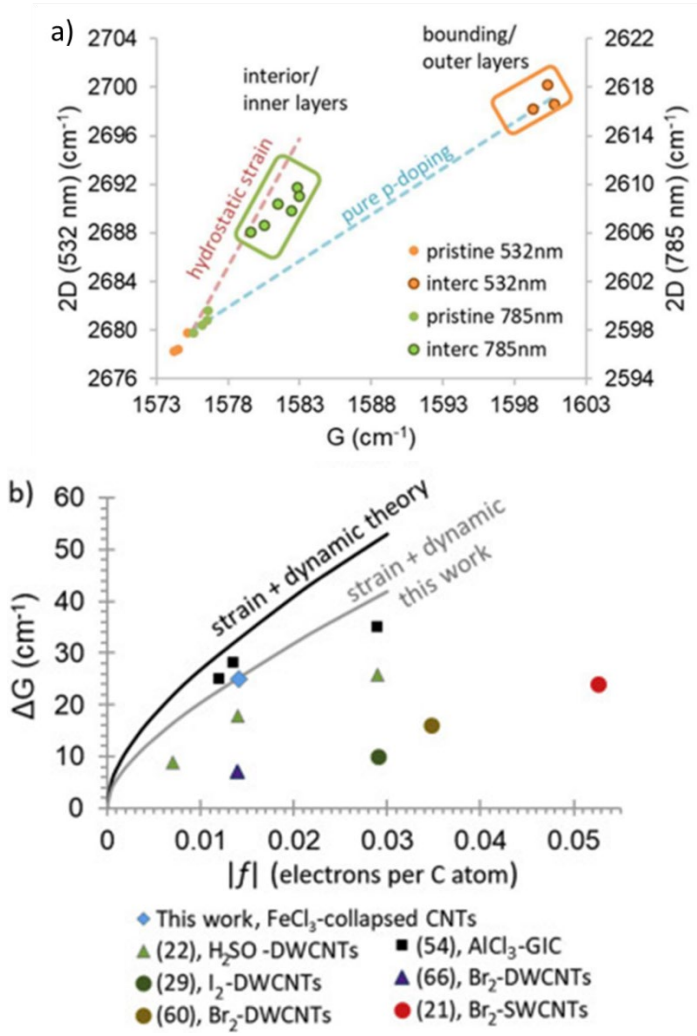


Figure 4. Determination of charge transfer upon intercalation from Raman spectra. a) Raman G-2D representation. Taking spectra with different laser lines enables separating the effect of intercalation on inner and outer layers. b) Representation of the parametrized curves of strain (with expanded lattice) plus dynamic effects (black) obtained theoretically, together with experimental data from this work (and proposed parametrized curve, in grey) and from literature.

### 6.3 Ultra-aligned CNT fibres from spun from liquid crystals

Fibres spun from liquid crystals are interesting model systems to study intercalation because of their extremely high degree of alignment, ultrahigh purity and are quasi-monodisperse composition. In this project, we started by studying the microstructure and properties of LC-

fibres subjected to different annealing treatments, together with collaborators from Rice University and the Korea Institute of Science and Technology.

The hierarchical structure of the fibres was reduced to dominant structure descriptors through the use of WAXS measurements. Fig. 5a presents the two-dimensional (2D) WAXS patterns of CNT fibers in pristine form and after annealing at 1700 and 2700 °C. As inferred from the equatorial (Fig. 5b) and meridional (inset) radial profiles, these annealing temperatures mark the main transformations. The starting material consists of highly aligned CNTs (full width at half maximum (FWHM) < 9°) in bundles with limited order and residual acid molecules. Annealing up to 1700 °C removed the acid molecules and induced CNT compaction, leading to strong interplanar *{hk0}* reflections and a smaller interlayer spacing. Annealing above 1700 °C resulted in a transition from CNT bundles to flat, elongated graphitic domains, similar to ribbons, observed by the sharpening of the (002) interlayer reflection and the emergence of strong {100} and {110} reflections. After annealing at 2700 °C, the material was highly graphitic, with interlayer spacing of 0.338 nm and {101} reflections indicating stacking order.

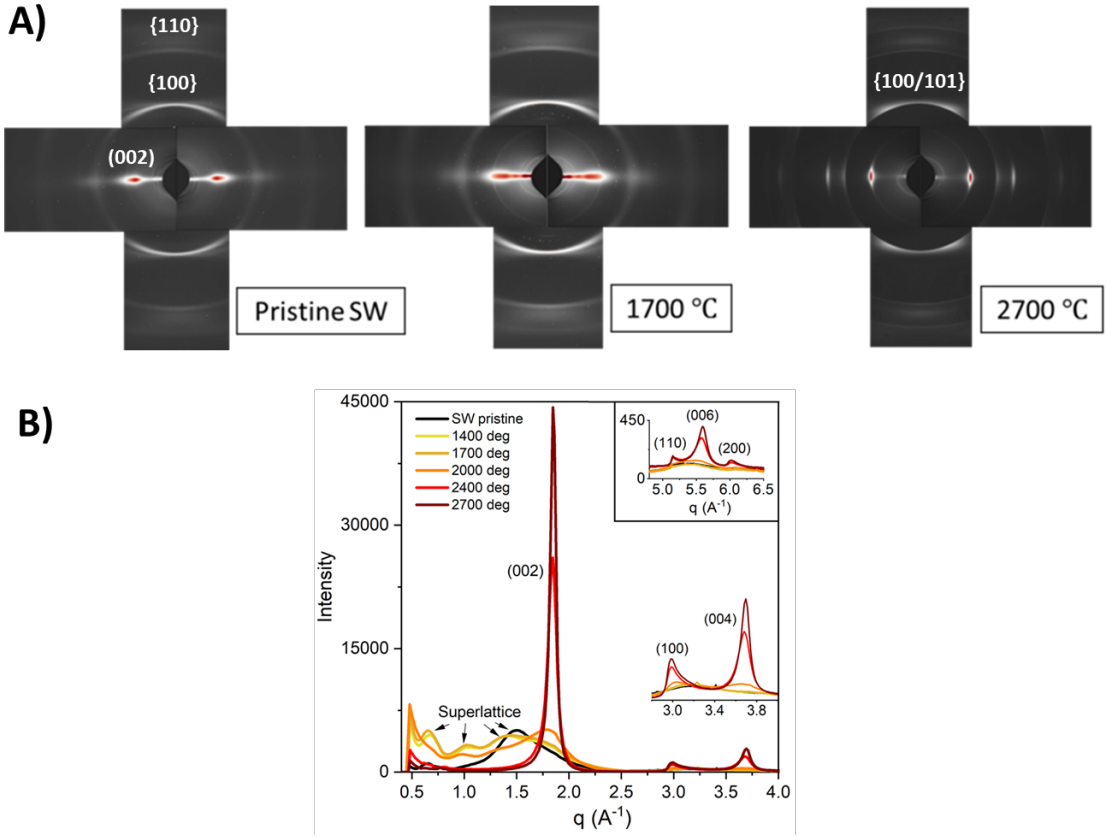


Figure 5. WAXS characterisation of LC-fibres in pristine form and annealed at different temperatures. A) 2D WAXS patterns. B) Radial profile along the equator and meridian (inset). Fibre axis vertical.

These materials cover a wide range of microstructures, spanning from fibres made of hexagonally closed-packed nanotubes with limited contact, to fibres of long planar stacks of graphitic domains with spacing close to Bernal graphite. It was found that after annealing, fibres of mixtures of SWNCTs and DWCNTs showed extraordinary longitudinal mechanical, electrical and thermal properties (Figure 6). Compared to carbon fibre, for example, they showed an usual

combination of high strength and stiffness (Figure 6b), as well as conductivity above many metals (Figure 6c-d). These properties stem from the macromolecular structure of the fibres, which enables realising simultaneously extremely long crystal length in the fibre direction and relatively small crystal size in the transverse direction to reduce brittleness.

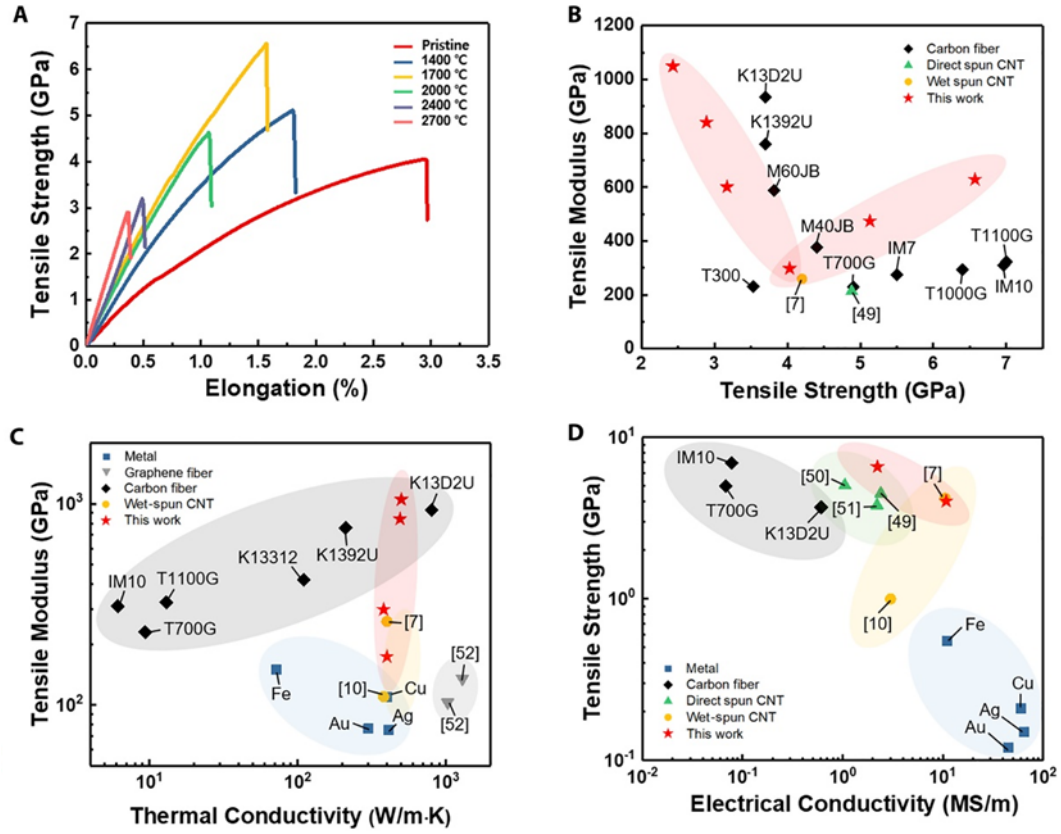


Figure 6. Longitudinal mechanical, electrical and thermal properties of CNT fibres annealed at different temperatures, and comparison to conventional carbon fibres and metals.

### 6.4 Br intercalation of ultra-aligned CNT fibres from spun from liquid crystals

Following exposure to $Br_2$ vapor, Br is introduced in the macroscopic DWCNT fiber (Figure 7) at the channels created by bundled CNTs. The internal structure of the material (Figure 7a), that is, the bundle structure, can be readily studied by observation of FIB-sliced cross sections of the fiber. Moreover, in HAADF mode Br atoms can be readily identified. As shown in Figure 7b, Br intercalates regularly at the interstitial channels defined by the hexagonally-packed DWCNTs. This arrangement is found throughout the whole cross section of the fiber in all regions of the sample analyzed by STEM in HAADF mode. The homogenous distribution of Br is further evidenced by EDX chemical mapping of bundle cross sections (Figure 7c).

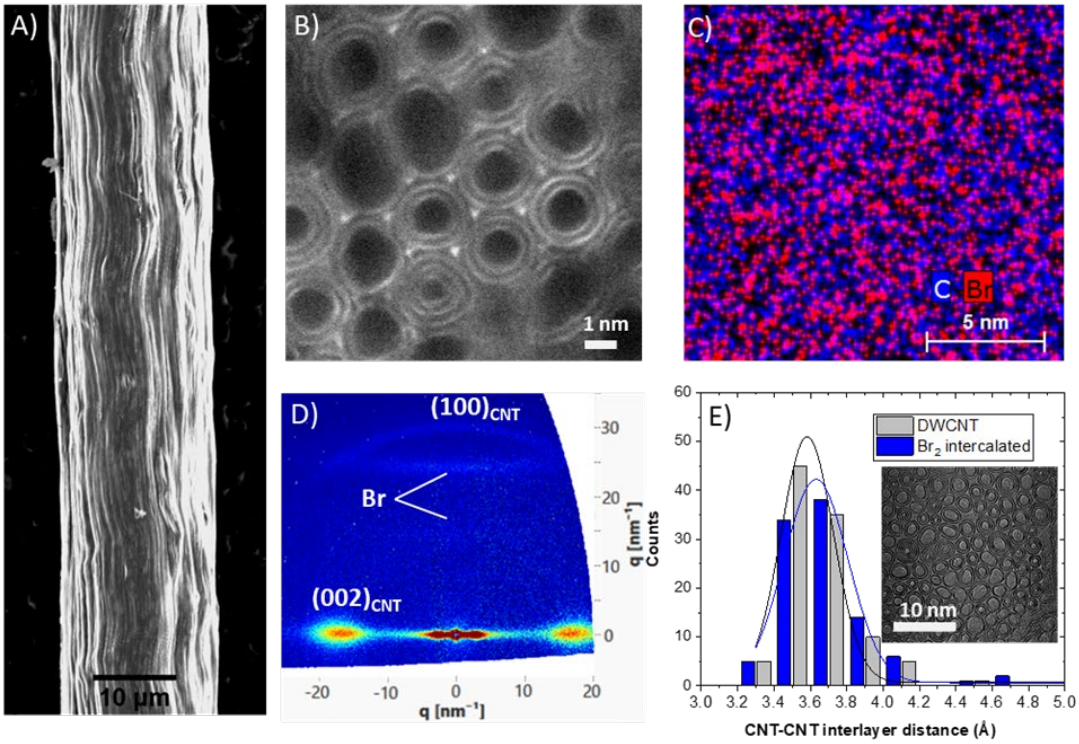


Figure 7. Structure of Br-intercalated fibers of DWCNT. a) SEM micrograph of an intercalated DWCNT fiber. b) HAADF STEM micrograph of the cross section of an intercalated fiber c) EDX chemical map showing widespread distribution of Br in the cross section. d) 2D WAXS pattern showing ordered domains of bromine species aligned with the fiber. e) Distribution of interlayer distance between adjacent CNTs from image analysis of HRTEM cross-sections, including Gaussian fit (inset: example of HRTEM micrograph).

2D WAXS measurements confirm the presence of Br and show that the resulting material corresponds to an intercalation compound with long range order of bromine species. As observed in the 2D pattern in Figure 7d, there are two strong meridional reflections not found in the pristine material and which correspond to ordered Br domains. The orientation of these reflections in the meridian, i.e., along the fiber direction, indicates that Br forms elongated periodic domains parallel to the DWCNTs, which can be visualized as Br “wires” nested in the CNT bundles. Figure 7e presents the gausisian distribution of interlayer distances between neighbouring CNTs before and after intercalation. The data show an average interlayer distance of 3.619 ± 0.198 Å in the pristine material and 3.706 ± 0.336 Å after intercalation, which indicate that there are no appreciable changes in DWCNTs separation, which has strong implications for bulk properties. The equatorial 2D WAXS patterns also confirm the intercalation model of Br wires nested in the channels between DWCNTs without disrupting interlayer distances. This confirms that Br does not intercalate between layers of the same DWCNT or directly between the contact surface of adjacent nanotubes, which contrast with the structure of GICs. Br intercalation in graphite increases separation between graphite layers to 7.04 Å, equivalent to a 100 % increase in the c axis for a stage 1 compound. In these DWCNTs, the changes in apparent diameter after Br intercalation are within sample variations, at less than 5 %. Using linear density measurement we could determine the mass fraction of Br to be 28.7 %. This corresponds to an intercalation compound with stoichiometry $C_{25}Br$.

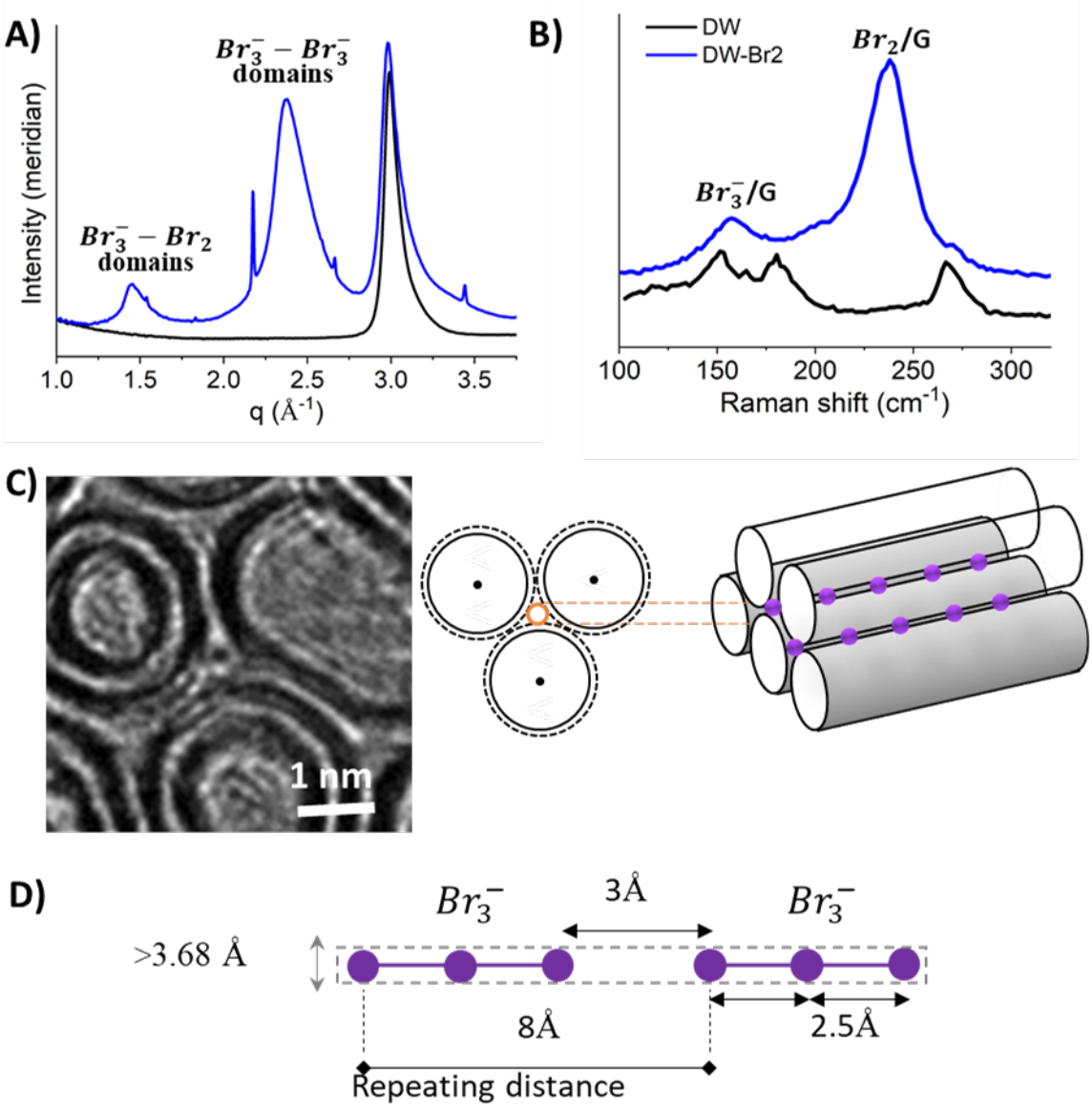


Figure 8. Structure of intercalated Br in fibers of DWCNTs. a) Meridional WAXS profiles showing Br features aligned parallel to the CNTs. b) Raman spectra region with redshifted vibrational features from $Br_3^-$ and $Br_2$, overlapped with RBMs in the intercalated sample. c) TEM micrograph and illustration of the interstitial channel in DWCNTs. d) Scheme showing a supramolecular Br structure forming "wires" along the bundle channels.

From analysis of the meridional WAXS profiles (Figure 8a), we assign the main reflection at q=2.35 Å$^{-1}$ with the periodic arrangment of linear $Br_3^-$-$Br_3^-$ chains aligned parallel to the nanotubes and separated by 3 Å. Such asignment is based on the corresponding distance (d=2π/q) of 2.67 Å being equal to a third of the repeating distance in the arrangement of anionic chains (Figure 8d). The presence of $Br_3^-$ has been previously proposed in Br-GICs.[22,23] The weaker feature at q=1.46 Å$^{-1}$ corresponds to tilted Br forming domains following the direction of the intersticies, i.e. of the bundles.

These results suggest that the structure of the intercalate in CNTICs is governed by the size of the interstitial channel.[24] Despite the lack of crystallographic registry in bundles of DWCNTs and the presence of multiple chiral angles, our results show that supramolecular organisation of bromine is possible in highly aligned CNTs and, thus, not directed by the atomic structure of the surrounding graphitic surface of the tubes. This contrasts with the view stemming from previous work on GICs which proposes that graphite crystallographic registry and commensurability with the Br intercalate lattice are required for long-range order intercalation of bromine.[22,23]

The basic structure proposed for intercalation compound is further verified by DFT simulations of bundles. Our simulations confirm the presence of the tribromide anion, which is arranged as periodic $Br_3^-$-$Br_3^-$ chains along the CNTs bundles, as appreciated in Figure 9. The anions form close to the surface of CNTs, precisely because it is the charge transfer that stabilizes them.[25] The confirmation of the presence of $Br_3^-$ also agrees with previous DFT simulations showing that the contact of iodine with CNTs leads to doping through the formation of charged iodide chains.[26] In the simulation, we can also appreciate perpendicular $Br_3^-$-$Br_2$ contacts, where the electrophilic $Br_2$ molecule interacts with the excess electronic density present in the $Br_3^-$ moiety, in both the terminal and central atoms. This is consistent with the literature regarding halogen-halogen interactions.[27]

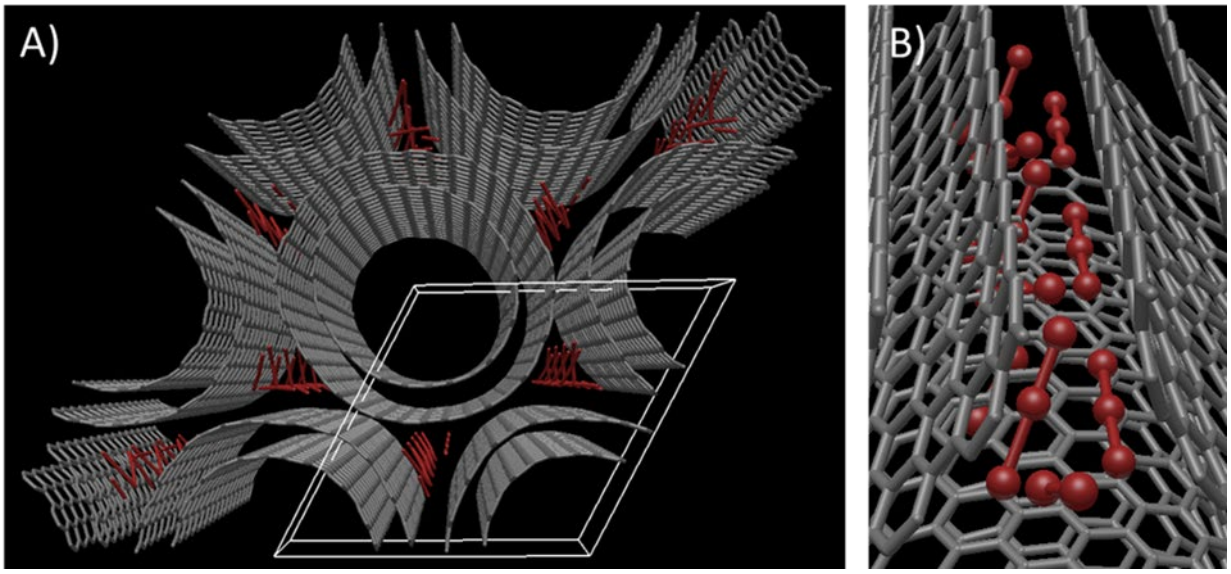


Figure 9. Simulation of CNT bundles with intercalated bromine. a) Equilibrium structure with ordered polybromides. b) Detailed sideline view of the ordering showing the linear arrangement for the $Br_3^-$ species, as well as tilted $Br_3^-$ and $Br_2$.

The calculation of Bader atomic charges evidences p-type doping occurring as a result of the addition of bromine to the CNTs. Our simulations show a displacement of electronic density from the carbon nanotubes toward $Br_3^-$ of 0.13 electrons per Br atom. In contrast, simulations that do not entail the formation of the $Br_3^-$ species only show a displacement of 0.04 electrons per atom. This highlights the importance of forming the $Br_3^-$ anion for the charge-carrying process.

### 6.5 Bulk properties of Br-intercalated DWCNT fibres

The final part of the project dealt with determining the bulk mechanical and electrical properties of these Br-intercalated fibres, and their relation to the structure resolved. The room-temperature longitudinal electrical conductivity increases by a factor of 8.4 to 10.68 $MSm^{-1}$ upon bromine intercalation, or normalized by specific gravity (SG), to 4.56 $MSm^{-1}SG^{-1}$. These values are at the high end of CNT fibers and in the top range reported for doped aligned fibers. They are similar to the in-plane conductivity of most GICs, above the conductivity of individual bundles of SWNTs,[28] and approach Cu and Al.

Through low-temperature transport measurements in the longitudinal and transverse directions, it was found that the intercalate reduces the tunneling-dominated resistance associated with transport between adjacent CNTs. This contrasts with the previous view in the field that intercalates exclusively act as a dopants that increase conductance of individual CNTs.

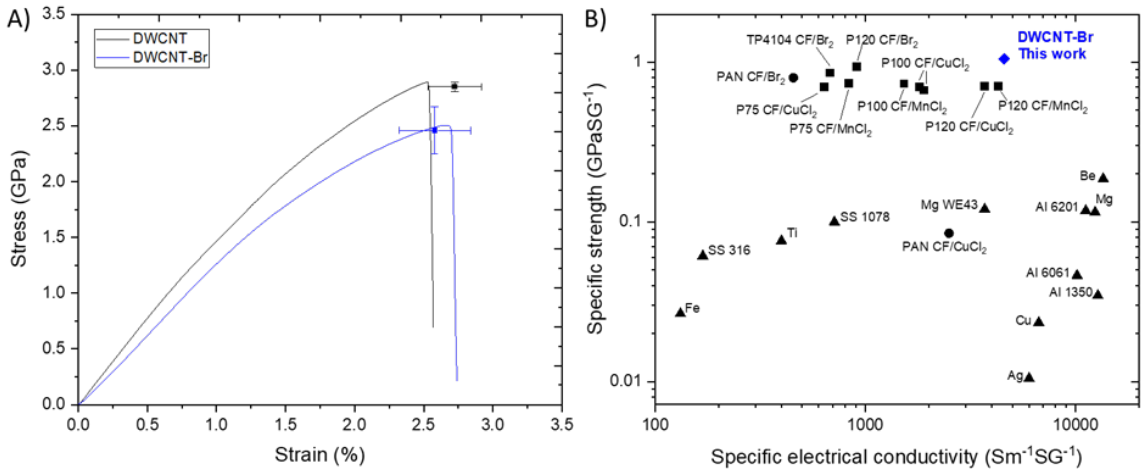


Figure 10. Longitudinal properties of Br-intercalated DWCNT fibers and comparison to other materials. a) Stress-strain curves showing minor changes in strength and modulus after intercalation. b) Plot of specific conductivity and specific strength of different intercalated compounds (mesophase pitch- and PAN-based CF intercalated with $Br_2$, $CuCl_2$ and $MnCl_2$) [29],[30,31] and reference metals, showing that combined low density, strength and conductivity can only be reached with CNTICs.

As shown in Figure 10a, the tensile properties of intercalated fibres are very similar to those of the pristine material, combining a high specific tensile strength with a relatively high strain-to-break (2.58 ± 0.26 %) and thus significant fracture energy. The gradual sloping from elasto-plastic deformation is evident in both materials. These results show that the presence of Br intercalate does not affect internal stress transfer. This is expected for the observed macromolecular structure of the intercalation compound, where Br intercalates at interstitial sites but does not change inter-tube spacing, thus not interfering with stress transfer in shear between adjacent CNTs. That is not the case for GICs and many CFs, in which changes in interlayer spacing and stress transfer through the intercalate layer change dramatically stress transfer perpendicular to the basal plane.

# 7 FUTURE WORK

The project demonstrated the formation of intercalation compounds of CNTs with a regular cross-section and unprecedented longitudinal order, essentially a continuous supramolecular structure of intercalate “wires” nested in conducting CNT bundles. Because the intercalate does not significantly change inter-tube separation, stress transfer between CNTs is not modified and the exceptional mechanical properties of the host CNT fibers are retained. The possibility to produce intercalation compounds with minimal disruption of the host lattice overcomes an inherent limitation in traditional layered GICs, making continuous, ordered anisotropic CNTICs a fascinating new family of materials. More efforts should be directed at synthesising the large library of possible CNT fibre intercalation compounds.

Future work would focus on introducing intercalates leading to a larger charge transfer that could thus increase longitudinal electrical conductivity beyond copper, a longstanding goal for nanocarbons. En route to this objective, it is of interest to perform transport measurements on smaller units of intercalated fibres to determine internal bundle conductance and inter-bundle charge transport resistance, which could then lead to a complete mesoscopic network model that bridges que nano and macroscopic scales.

Another area of interest is to determine the detailed structure and properties of the intercalate “wires” nested in the bundles, including the possibility that suitable intercalate may exhibit one-dimensional electronic structure and transport features. Furthermore, the ordered intercalated structures obtained suggest the formation of new metamaterial structures. This will be the subject of a follow-up proposal.

# 8 REFERENCES

[1] Koziol K, Vilatela J, Moisala A, Motta M, Cunniff P, Sennett M, et al. High-performance carbon nanotube fiber. Science (80- ) 2007;318. https://doi.org/10.1126/science.1147635.

[2] Senokos E, Reguero V, Palma J, Vilatela JJ, Marcilla R. Macroscopic fibres of CNTs as electrodes for multifunctional electric double layer capacitors: From quantum capacitance to device performance. Nanoscale 2016;8. https://doi.org/10.1039/c5nr07697h.

[3] Gspann TS, Juckes SM, Niven JF, Johnson MB, Elliott JA, White MA, et al. High thermal conductivities of carbon nanotube films and micro-fibres and their dependence on morphology. Carbon N Y 2017;114:160–8. https://doi.org/10.1016/J.CARBON.2016.12.006.

[4] Dresselhaus MS, Dresselhaus G. Intercalation compounds of graphite. Adv Phys 2002;51:1–186. https://doi.org/10.1080/00018730110113644.

[5] Novko D, Zhang Q, Kaghazchi P. Nonadiabatic Effects in Raman Spectra of AlCl4− -graphite Based Batteries. Phys Rev Appl 2019;12:024016.

https://doi.org/10.1103/PhysRevApplied.12.024016.

[6] Endo, M., Chieu, T. C., Timp, G., & Dresselhaus MS. Properties of acceptor intercalated graphite fibers. Synth Met 1983;8:251–60.

[7] Liu Y, Xu Z, Zhan J, Li P, Gao C. Superb Electrically Conductive Graphene Fibers via Doping Strategy. Adv Mater 2016;28:7941–7. https://doi.org/10.1002/adma.201602444.

[8] Zhao W, Tan PH, Liu J, Ferrari AC. Intercalation of few-layer graphite flakes with FeCl3: Raman determination of Fermi level, layer by layer decoupling, and stability. J Am Chem Soc 2011;133:5941–6. https://doi.org/10.1021/ja110939a.

[9] Herold A. Research on the insertion compounds of graphite. Bull Soc Chim Fr 1955.

[10] Hérold A. Synthesis of graphite intercalation compounds. In: Legrand AP, Flandrois S, editors. Chem. Phys. intercalation. NATO ASI S, Boston: Springer; 1987, p. 3–45. https://doi.org/10.1007/978-1-4757-9649-0_1.

[11] Wang L, Zhu Y, Guo C, Zhu X, Liang J, Qian Y. Ferric chloride-graphite intercalation compounds as anode materials for Li-ion batteries. ChemSusChem 2014;7:87–91. https://doi.org/10.1002/cssc.201300874.

[12] Müller-Warmuth, W., & Schöllhorn R (Eds. . Progress in intercalation research. vol. 17. vol. 17. Springer Science & Business Media; 2012. https://doi.org/10.1007/978-94-011-0890-4.

[13] Su SR, Oblas DW. The intercalation of micron-size graphite powder with anhydrous ferric chloride. Carbon N Y 1987;25:391–4. https://doi.org/10.1016/0008-6223(87)90010-8.

[14] Underhill C, Leung SY, Dresselhaus G, Dresselhaus MS. Infrared and Raman spectroscopy of graphite-ferric chloride. Solid State Commun 1979;29:769–74. https://doi.org/10.1016/0038-1098(79)90158-3.

[15] Luski S, Ohana I, Selig H. Graphite fibers intercalated with AsF5: A comparison of PAN and pitch-based fibers. Carbon N Y 1987;25:799–801. https://doi.org/10.1016/0008-6223(87)90154-0.

[16] Chacón-Torres JC, Wirtz L, Pichler T. Raman spectroscopy of graphite intercalation compounds: Charge transfer, strain, and electron-phonon coupling in graphene layers. Phys Status Solidi 2014;251:2337–55. https://doi.org/10.1002/pssb.201451477.

[17] Lee JE, Ahn G, Shim J, Lee YS, Ryu S. Optical separation of mechanical strain from charge doping in graphene. Nat Commun 2012;3:1–8. https://doi.org/10.1038/ncomms2022.

[18] Mueller NS, Heeg S, Alvarez MP, Kusch P, Wasserroth S, Clark N, et al. Evaluating arbitrary strain configurations and doping in graphene with Raman spectroscopy. 2D Mater 2017;5:015016. https://doi.org/10.1088/2053-1583/aa90b3.

[19] Puech P, Hu T, Sapelkin A, Gerber I, Tishkova V, Pavlenko E, et al. Charge transfer between carbon nanotubes and sulfuric acid as determined by Raman spectroscopy. Phys Rev B 2012;85. https://doi.org/10.1103/PhysRevB.85.205412.

[20] Lazzeri M, Mauri F. Nonadiabatic Kohn anomaly in a doped graphene monolayer. Phys Rev Lett 2006;97:266407. https://doi.org/10.1103/PhysRevLett.97.266407.

[21] Tristant D, Zubair A, Puech P, Neumayer F, Moyano S, Headrick RJ, et al. Enlightening the ultrahigh electrical conductivities of doped double-wall carbon nanotube fibers by Raman spectroscopy and first-principles calculations. Nanoscale 2016;8:19668–76.

[22] Eklund PC, Kambe N, Dresselhaus G, Dresselhaus MS. In-plane intercalate lattice modes in graphite-bromine using Raman spectroscopy. Phys Rev B 1978;18:7069–79. https://doi.org/10.1103/PhysRevB.18.7069.

[23] Ghosh D, Chung DDL. Two-dimensional structure of bromine intercalated graphite. Mater Res Bull 1983;18:1179–87.

[24] Pichler T, Liu X, Knupfer M, Fink J. Electronic properties of intercalated single-wall carbon nanotubes and C60 peapods. New J Phys 2003;5:156. https://doi.org/10.1088/1367-2630/5/1/156.

[25] Sedelnikova O V., Ewels CP, Pinakov D V., Chekhova GN, Flahaut E, Okotrub A V., et al. Bromine polycondensation in pristine and fluorinated graphitic carbons. Nanoscale 2019;11:15298–306. https://doi.org/10.1039/C9NR01922G.

[26] Zubair A, Tristant D, Nie C, Tsentalovich D, Headrick R, Pasquali M, et al. Charged iodide in chains behind the highly efficient iodine doping in carbon nanotubes. Phys Rev Mater 2017;1. https://doi.org/10.1103/PhysRevMaterials.1.064002.

[27] Reddy CM, Kirchner MT, Gundakaram RC, Padmanabhan KA, Desiraju GR. Isostructurality, Polymorphism and Mechanical Properties of Some Hexahalogenated Benzenes: The Nature of Halogen···Halogen Interactions. Chem – A Eur J 2006;12:2222–34. https://doi.org/https://doi.org/10.1002/chem.200500983.

[28] Bulmer JS, Kaniyoor A, Elliott JA. A Meta-Analysis of Conductive and Strong Carbon Nanotube Materials. Adv Mater 2021;33:2008432. https://doi.org/https://doi.org/10.1002/adma.202008432.

[29] Błażewicz S, Touzain P. Properties of metal-chlorides intercalated graphite fibres. Ceram Int 1998;24:111–5. https://doi.org/https://doi.org/10.1016/S0272-8842(96)00088-0.

[30] Murday JS, Dominguez DD, Moran JA, Lee WD, Eaton R. An assessment of graphitized carbon fiber use for electrical power transmission. Synth Met 1984;9:397–424. https://doi.org/https://doi.org/10.1016/0379-6779(84)90007-9.

[31] Fischbach DB, Arnold MG, Flandrois S. Tensile properties of intercalated pitch mesophase carbon fibers. Synth Met 1989;34:733–8. https://doi.org/https://doi.org/10.1016/0379-6779(89)90467-0.